Polarization evolution on the higher-order Poincaré sphere via photonic Dirac points

Wenhao Xu,[1] Shizhen Chen,[1] Shuangchun Wen,[2] and Hailu Luo[1,2,*]

[1]*Laboratory for Spin Photonics, School of Physics and Electronics, Hunan University, Changsha 410082, China*

[2]*Key Laboratory for Micro-/Nano-Optoelectronic Devices of Ministry of Education, School of Physics and Electronics, Hunan University, Changsha 410082, China*

(Received 8 December 2020; accepted 21 June 2021; published 6 July 2021)

In this work, we report a general reflection model to describe the reflected behaviors of a Gaussian beam near photonic Dirac point at the optical interface. With spin polarized electromagnetic waves strikes near the single Dirac point on Dirac material interface, vortical phase distribution and spin inversion are demonstrated for reflected state, and we further develop a higher-order Poincaré sphere to describe the evolution of polarization states. It is possible to generate any desired Poincaré vortex beam on the sphere by modulating the incident polarization state of light. Moreover, we discuss the case of normal incidence around two adjacent Dirac points, reflection spectrum involves a couple of spin flip vortices corresponding to two points with the corresponding topological invariants, which are consistent with the Berry curvature and topological charge. These results can be extended to similar hyperbolic metamaterials with degenerate point, and inspire a different perspective for manipulating polarized vortex beam with photonic Dirac point.

DOI: 10.1103/PhysRevA.104.013504

I. INTRODUCTION

In photonics, the fourfold degeneracy of Dirac point is functioning as monopoles of Berry flux with topological charges defined by the Chern numbers, and Dirac point can be viewed as two overlapping Weyl points with opposite topological charges. Recently, Dirac points [1,2], Weyl points [3–7], and nodal lines [8] have been realized in optical systems with broken inversion symmetry such as optical lattices [9,10], classical acoustic [11–13], photonic crystals [14–16] as well as plasmonic structures [17,18]. These application of photonic degenerate point at topological metamaterials interface has led to some new paradigms in developing photonic devices with robust properties, such as manipulation of optical angular momenta with photonic Weyl systems [19], robust counter-propagating edge states [20], topological photonic routing in a bearded-stack interface [21], and topological vortex lasing by spin-momentum locking [22].

Recently the concept of the higher-order Poincaré sphere was introduced as a theoretical framework for describing the total angular momentum of light, both spin and angular components [23,24]. Similar to the geometric representation of homogeneous polarizations on Poincaré sphere, a prominent geometric representation of the vector beams is provided by the so-called higher-order Poincaré sphere, which describes higher-order states of polarization of generalized vector vortex beams [25,26], in contrast to the Poincaré sphere, which is a geometric representation of all possible states of polarization [27]. In geometrical representation rule, phase evolution is demonstrated on the higher-order Poincaré sphere [28,29].The phase is geometric in nature and differs significantly from a dynamic phase, which is proportional to light's total angular momentum. This state evolution will provide an advantage solution to create optical qubits and improve the simplify optical analog computation. The emergence of topological materials provide an important opportunity to reexamine the polarization evolution via photonic Dirac points. Nevertheless, the evolution of polarization state reflected at topological interface have not been given a distinct representation.

In this paper, we establish a general model to describe the reflected behaviors of a Gaussian beam at the interface of uniaxial metamaterials with homogeneous effective electromagnetic properties. Based on calculations with a rigorous wave theory, we show that when a circular polarization light beam with a particular spin incident on individual Dirac point, the unique polarization-dependent interactions between light and the medium can convert the spin character of input, endow the reflected beam with an additional vortex phase. The reflected polarization states are sketched by the point-to-point conversion from the fundamental Poincaré sphere to the higher-order Poincaré sphere. Moreover, we extend the reflected module to the normal incidence on paired Dirac points, there are two vortex structures predictably appear at the position of paired Dirac points. By means of interference pattern, the central of phase distribution possess a topological charge as ± 2, while other single Dirac point corresponding to ± 1. Intriguingly, the reflectance spectrum at the interface. As a result, the representation of the higher-order Poincaré sphere has become an important technique to deal with the polarization evolution in other optical systems with degeneracy point, and provides a deeper insight into physical mechanisms.

II. GENERAL MODEL FOR REFLECTION FIELD NEAR PHOTONIC DIRAC POINT

Here, we first use hyperbolic electromagnetic structure to construct Dirac points, the general permittivity and

*hailuluo@hnu.edu.cn

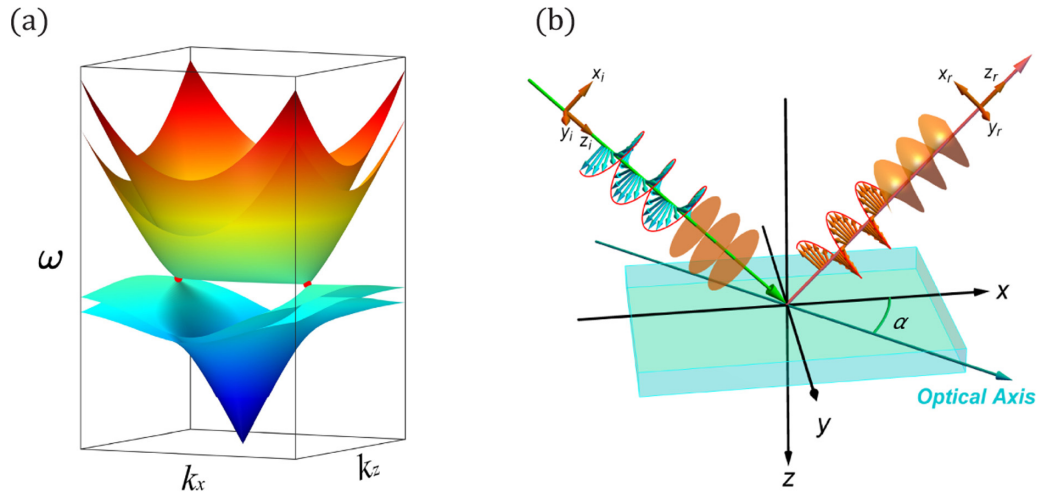

FIG. 1. (a) The effective bulk band structure of Dirac metamaterials on a wave vector plane. Two bands are nearly overlapping with each other, and there are fourfold band degeneracies at two points (marked by the red spheres), which are symmetrically placed. (b) Schematic illustrating the wave reflected vortex beams near the Dirac point at the interface of Dirac hyperbolic metamaterials. We set ***xy*** plane as an interface between air ($z > 0$) and Dirac metamaterials ($z < 0$) characterized by $\boldsymbol{\varepsilon}$, $\boldsymbol{\mu}$.

permeability tensors of medium have the anisotropic form as $\boldsymbol{\varepsilon} = \varepsilon_0 \mathrm{diag}\{\varepsilon_x, \varepsilon_y\, \varepsilon_z\}$ and $\boldsymbol{\mu} = \mu_0 \mathrm{diag}\{\mu_x, \mu_y\, \mu_z\}$, respectively. The presence of resonance along the x direction for both permittivity and permeability indicates that there exist two bulk plasmon modes [1,30,31], a longitudinal electric mode, and a longitudinal magnetic mode, $\varepsilon_x = 1 + f_1\omega_0^2/(\omega_0^2 - \omega^2)$, $\mu_x = 1 + f_2\omega^2/(\omega_0^2 - \omega^2)$, where ω_0 indicates the resonance frequency and coefficients f_1 and f_2 are constants determined by the structure parameters, which are adjustable, $f_2 = 1 - 1/(1 + f_1)$. Then we assume $\varepsilon_z = \varepsilon_y$, $\mu_z = \mu_y$ are constants. The dispersion relations of Dirac metamaterials can be deduced from corresponding characteristic equation (see in Appendix A). Figure 1(a) shows the band structure of bulk states in the $k_x - k_z$ plane, where two bands are nearly overlapping with each other. In the x direction in momentum space, there are two fourfold degeneracy points named photonic Dirac points symmetrically displaced, as marked with the red spheres.

Let us consider that a Gaussian beam of frequency ω impinges at an angle θ on the interface between vacuum and the medium. Benefiting from the translational invariance nature of the Dirac metamaterials, the incident beam is not required to be aligned to a certain position on the media. $k_i = \omega/\sqrt{\varepsilon_0\mu_0} = \omega/c$ is the incident vector, c is the speed of light, and we assume the incident wave vector lies on the ***xz*** plane, as shown in Fig. 1(b). We set ***xy*** plane as an interface between vacuum ($z > 0$) and medium ($z < 0$) characterized by $\boldsymbol{\varepsilon}$, $\boldsymbol{\mu}$. Consider a plane wave of frequency incident from vacuum, making an angle θ_i with respect to the interface normal.

However, for a Gaussian beam with finite beam width incident to the interface, the arbitrary wave vector of the beam should be taken into account. We assume that the wave function in momentum space can be specified by the following expression:

$$|\Phi\rangle = \frac{w_0}{\sqrt{2\pi}} \exp\left[-\frac{w_0^2\left(k_{ix}^2 + k_{iy}^2\right)}{4}\right], \tag{1}$$

where w_0 is the width of wave function. The total wave function is made up of the packet spatial extent and the polarization state. We noted that k_{ix} and k_{iy} respects the x and y components of arbitrary vector relative to beam center ($k_{ix} = k_{iy} = 0$), respectively. Naturally, the behavior of arbitrary wave vector can obtain by Cartesian coordinate transformation of center vector.

We first introduced a optical axis vector $\mathcal{I} = \cos\alpha\,\hat{\mathbf{x}} + \sin\alpha\,\hat{\mathbf{y}}$, and α is an angle of optical axis relative xz plane, where $\hat{\mathbf{x}}$ and $\hat{\mathbf{y}}$ are unit vectors along the x and y positive axes. With $\Delta\varepsilon = \varepsilon_x - \varepsilon_y$ and $\Delta\mu = \mu_x - \mu_y$, the coordinate transformation can be embedded into the anisotropic permittivity tensor as:

$$\boldsymbol{\varepsilon_r} = \begin{vmatrix} \varepsilon_y + \cos^2\alpha\Delta\varepsilon & \sin\alpha\cos\alpha\Delta\varepsilon & 0 \\ \sin\alpha\cos\alpha\Delta\varepsilon & \varepsilon_y + \sin^2\alpha\Delta\varepsilon & 0 \\ 0 & 0 & \varepsilon_y \end{vmatrix}, \tag{2}$$

$$\boldsymbol{\mu_r} = \begin{vmatrix} \mu_y + \cos^2\alpha\Delta\mu & \sin\alpha\cos\alpha\Delta\mu & 0 \\ \sin\alpha\cos\alpha\Delta\mu & \mu_y + \sin^2\alpha\Delta\mu & 0 \\ 0 & 0 & \mu_y \end{vmatrix}. \tag{3}$$

In the following we can apply the Maxwell equations and boundary conditions to educe the general reflection coefficients in Dirac metamaterials without taking arbitrary vector into account [32], as schematically shown in Appendix B. Second, we should note that the arbitrary incident vector of Gaussian beam form an angle with incident xz plane, thus the arbitrary wave vector can be indicated by α. For the case of Gaussian beam incident near the single Dirac point, the modified Fresnel¡¯s coefficients are given by using the paraxial approximation in momentum space [33,34].

The polarization states on the fundamental Poincaré sphere with the azimuthal and polar angles (Θ, Φ) can be written as:

$$|\psi_{in}\rangle = \cos\left(\frac{\Theta}{2}\right)\exp\left(i\frac{\Phi}{2}\right)|L\rangle + \sin\left(\frac{\Theta}{2}\right)\exp\left(-i\frac{\Phi}{2}\right)|R\rangle. \tag{4}$$

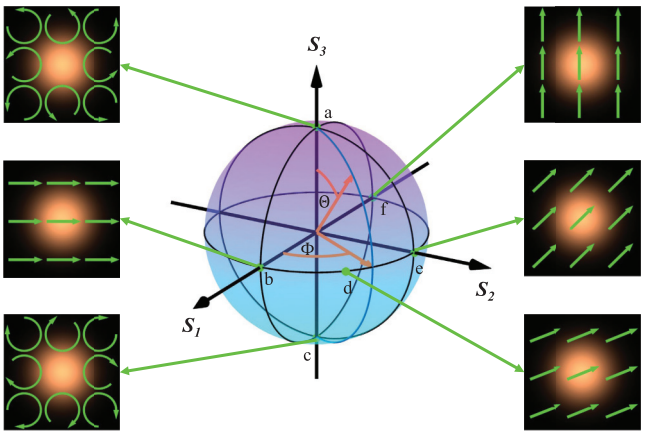

FIG. 2. Schematic illustrating the homogeneous polarization state distribution on the fundamental Poincaré sphere. The north and south poles represent left- and right-handed circular polarization, respectively. Any polarization state on the sphere can be regarded as their linear combination. The signs of a ∼ f are the reference points with coordinates (0, 0, 1), (1, 0, 0), (0, 0, −1), $(\sqrt{2}/2, \sqrt{2}/2, 0)$, (0, 1, 0), and (−1, 0, 0). We set an incident beam with waist radius $w_0 = 100\lambda$, and $\lambda = 2\pi c/\omega$.

Here, $|L\rangle = (\hat{x} + i\hat{y})/\sqrt{2}$ and $|R\rangle = (\hat{x} - i\hat{y})/\sqrt{2}$ are left-handed polarization (LCP) and right-handed circular polarization (RCP), respectively. The intensity distribution and uniform polarization of the beam on the fundamental Poincaré sphere are plotted in Fig. 2.

In our scheme, the reflected polarization states related to the incident polarization states can be described by the following matrix $\mathcal{M}^{(r)}$:

$$\mathcal{M}^{(r)} = \begin{bmatrix} r_{ll} & r_{lr} \\ r_{rl} & r_{rr} \end{bmatrix}, \tag{5}$$

where $r_{ll}, r_{lr}, r_{rl}, r_{rr}$ represent the Fresnel coefficients under CP basis near the Dirac points, and the expression of reflection coefficients are as follows:

$$r_{ll} = \frac{1}{2}\left[(r_{pp} - r_{ss}) - \frac{k_{rx}}{k}(r'_{pp} - r'_{ss}) - i\frac{k_{ry}}{k}(r'_{ps} - r'_{sp})\right], \tag{6}$$

$$r_{rr} = \frac{1}{2}\left[(r_{pp} - r_{ss}) - \frac{k_{rx}}{k}(r'_{pp} - r'_{ss}) + i\frac{k_{ry}}{k}(r'_{ps} - r'_{sp})\right], \tag{7}$$

$$r_{lr} = \frac{1}{2}\left[(r_{pp} + r_{ss}) - \frac{k_{rx}}{k}(r'_{pp} + r'_{ss}) - i\frac{k_{ry}}{k}(r'_{ps} - r'_{sp})\right], \tag{8}$$

$$r_{rl} = \frac{1}{2}\left[(r_{pp} + r_{ss}) - \frac{k_{rx}}{k}(r'_{pp} + r'_{ss}) + i\frac{k_{ry}}{k}(r'_{ps} - r'_{sp})\right]. \tag{9}$$

Obviously, the existence of crossing reflected coefficients generate the reflected field with opposite spin property. The spin-maintained and spin-reversal beams are referred to as normal and abnormal modes, respectively. This means that even though the incident beam exhibits a pure spin, the reflected beam can still contain a spin-reversal abnormal component which comes from the effective anisotropy interface [35]. As shown in Figs. 3(a) and 3(b), when incident angle meet the photonic Dirac point, those related reflection coefficients reached the critical value, $r_{pp} = r_{ss}$, $r'_{pp} = r'_{ss}$, $r'_{ps} = -r'_{sp}$, so $r_{ll} = r_{rr} = 0$, r_{lr} and $r_{rl} \neq 0$, which means all normal reflected component (spin-maintained) disappeared and the only abnormal reflected component (spin-reversal) were retained. Significantly, two crossing coefficients r_{lr} and r_{rl} carries the equal amplitude and opposite phase with photonic Dirac point (see Appendix C for details). When a circularly polarized incident beam, say LCP case, shines on the metasurface, the output reflected beam is completely converted to abnormal mode beam with opposite handedness, i.e., right-handed, which carry an additional phase, and the parallel situation exists on RCP incidence.

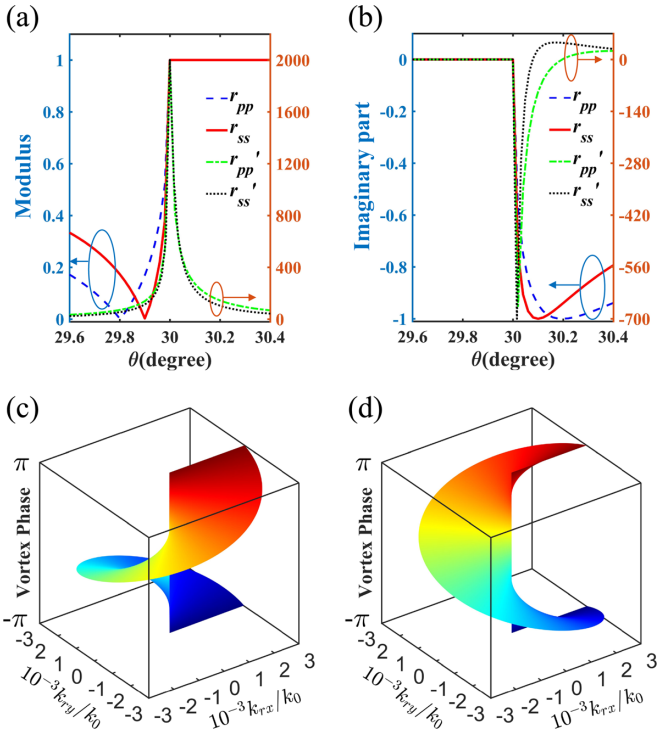

FIG. 3. The reflection amplitude (a) and imaginary part of reflection coefficients (b) near the Dirac point ($\theta \to 30°$). The parameters r'_{pp} and r'_{ss} also as the function of incident angle. (c) and (d) show phase distribution of left-handed and right-handed circular polarizations light incidence in momentum space, respectively. We set an incident beam with frequency $\omega = \omega_D(1 + 0.002)$, parameters for the Dirac metamaterials are chosen as $\varepsilon_y = \mu_y = 0.5$, the resonance frequency $\omega_0 = 10^{14}$ Hz and structural coefficients $f_1 = 1$.

III. HIGHER-ORDER POINCARÉ SPHERE VIA PHOTONIC DIRAC POINT

To further analyze the underlying physics, we reexamine the matrices $\mathcal{M}^{(r)}$ under the paraxial-wave approximation, we have $r_{lr} \approx r'_{pp}(1 + i\phi_v)$, $\phi_v = r'_{ps}k_{ry}/r'_{pp}k_{rx}$. Therefore, the

matrix $\mathcal{M}^{(r)}$ now reads:

$$\mathcal{M}^{(r)} \approx \begin{bmatrix} 0 & r'e^{-i\phi_v} \\ r'e^{+i\phi_v} & 0 \end{bmatrix}, \tag{10}$$

Here ϕ_v is a k_x-k_y-dependent geometric phase originated from the polarization vector of the central plane wave and the noncentral ones inside the beam. In essence, this Berry phase comes from the topological structure of the beam itself, which is an unobservable quantity. Only the phase difference between the final state and the initial state of the beam is an observable quantity. For the abnormal mode, the phase difference is because of the spin flip; for the normal mode, the phase difference is zero. With incident angle point approaching the single Dirac point, the coefficients $r'_{ps}/r'_{pp} \to 1$. Thus the final phase of the abnormal mode and the normal mode is

$$\Psi_B = \Psi_B^r - \Psi_B^i = 2\sigma\pi \tag{11}$$

$\sigma \in \{+, -\}$ denote the left- and right-handed circular polarizations. As shown in Figs. 3(c) and 3(d), the phase difference show that generation of reflected vortex beam near the Dirac point at the interface and the phase distribution are precisely correspond the topological charge of ± 1.

The similar result of reflected vortex beam around the Dirac point first reported in Ref. [1], and they obtained the physical picture by solving for the eigenstates of the effective Hamiltonian [1,4,5], pointed out that laid the foundation for unveiling the connection between intrinsic physics and global topology in electromagnetism. While it should be noted that vortex structure in our scheme derived from reflection theory of electromagnetic waves based on paraxial approximation and coordinate transformation. The reflection model not only provide guidance on generation of vortex beam, but also reveals polarization evolution with distinct physical picture.

After substituting Eq. (4) into Eq. (10), the reflected states near the photonic Dirac point can be described by higher-order Poincaré sphere:

$$|\psi_{\text{out}}\rangle = \cos\left(\frac{\Theta_1}{2}\right)\exp\left(i\frac{\Phi_1}{2}\right)|L_1\rangle + \sin\left(\frac{\Theta_1}{2}\right)\exp\left(-i\frac{\Phi_1}{2}\right)|R_1\rangle, \tag{12}$$

where

$$|L_1\rangle = \frac{\sqrt{2}}{2}(\hat{x} + i\hat{y})\exp(-i\phi_v), \tag{13}$$

$$|R_1\rangle = \frac{\sqrt{2}}{2}(\hat{x} - i\hat{y})\exp(+i\phi_v). \tag{14}$$

The azimuthal phase factor $\exp(\pm i\ell\phi_v)$ is the vortex phase, which is associated with orbital angular momentum of $\pm\hbar$ per photon. The relations $\Theta_1 = \pi - \Theta$, $\Phi_1 = -\Phi$ indicate we can realize the vortex polarization states by the point-to-point conversion from the fundamental Poincaré sphere to the higher-order Poincaré sphere, see in Fig. 4.

IV. REFLECTION FIELD AND CHERN NUMBER NEAR PAIRED DIRAC POINTS

In previous research about single Dirac point, we can definitely see photonic Dirac points are linked to the vortex photonics with topological charge as ± 1. However, photonic Dirac points are known to occur in pairs in photonic graphene and other similar metamaterials [36,37], which are due to preserve time-reversal symmetry. So it was short comprehensive to discuss a single Dirac point affects reflected beam. Now for simultaneously thinking about the influence of paired Dirac points, we consider normal incidence of a Gaussian beam at the surface with two adjacent Dirac points, see in Fig. 5.

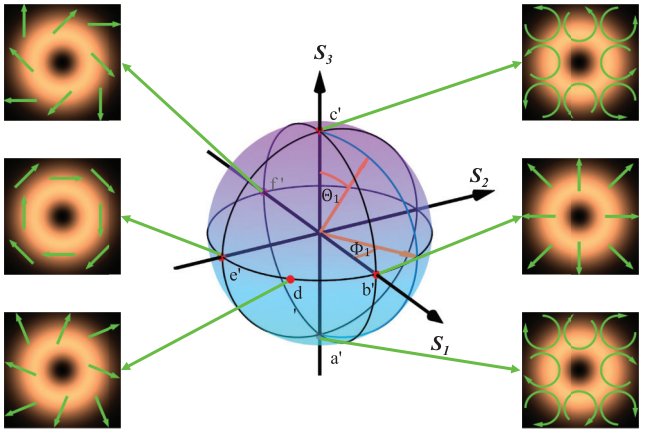

FIG. 4. The higher-order Poincaré sphere representation of the reflected field near the Dirac point illustrating the local polarization vectors states at various positions on the sphere. The location of six points a′ ∼ f′ on the sphere with coordinates (0, 0, −1), (1, 0, 0), (0, 0, 1), ($\sqrt{2}/2$,-$\sqrt{2}/2$, 0), (0, −1, 0), and (−1, 0, 0), which correspond to points a ∼ f on the fundamental sphere. The incident frequency is chosen as $\omega = \omega_D(1 + 10^{-12})$ and incident angle is chosen as $\theta = 30^\circ$. Parameters for the Dirac metacrystal are chosen as $\varepsilon_y = \mu_y = 0.5$, the resonance frequency $\omega_0 = 10^{14}$ Hz and structural coefficients $f_1 = 1$.

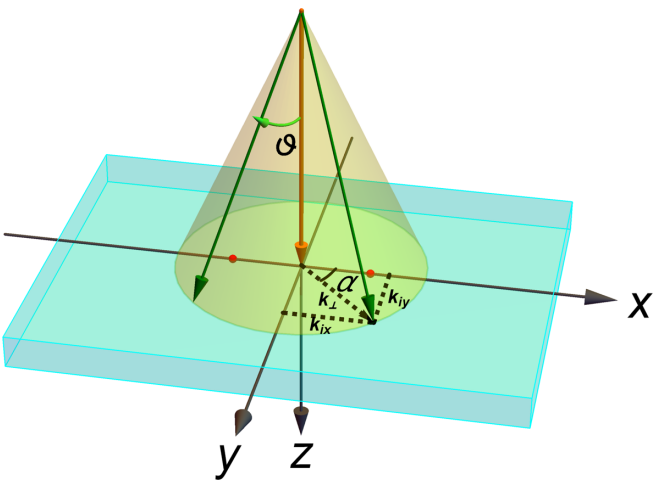

FIG. 5. Illustration of the Gaussian beam vertically incident at the interface of Dirac metamaterials with a paired Dirac points, which are placed center in momentum space. ϑ is the propagation angle of the plane wave components in the spherical coordinate system, $k_\perp = \sqrt{k_{ix}^2 + k_{iy}^2}$ is the transverse wave vector. Combining the unit incident plane vector $\mathcal{I}$, thus the angle α can be indicated by arbitrary wave vector: $\cos\alpha = k_{ix}/k_\perp$, $\sin\alpha = k_{iy}/k_\perp$.

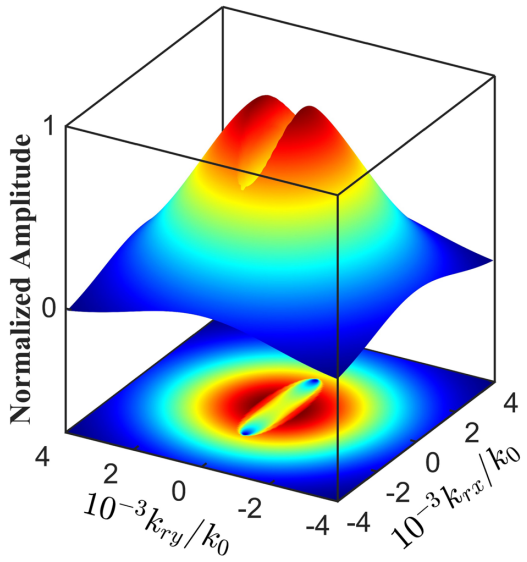

FIG. 6. Normalized reflectance amplitude and two-dimensional (2D) contour of left-handed circular polarization beam vertically incident at the interface with paired Dirac points.

Substituting the relationship of wave vectors into general expressions of Fresnel coefficients Eqs. (B6)–(B9) in Appendix B, we can get the corresponding reflection field concisely. For normal incident Gaussian beam, the behaviors of the reflection coefficients are nearly the same as the abnormal case. Only two crossing components r_{lr} and r_{rl} carry the phase information, while the other two components r_{ll} and r_{rr} do not supply any phase and contribute to normal reflections. The output spectrums with paired photonic Dirac point under left-handed polarized initial states are plotted in Fig. 6, intensity and topological phases of reflected field generate the correspondence with paired Dirac points in momentum space, which can be regarded as two vortices moving towards the center.

To further elucidate the topological behavior of designed Dirac metamaterials, we introduce Berry phase and topological charge (Chern number) to reveal the reflection near Dirac points. In the transmission process from an isotropic system (air) to a double hyperbolic system (Dirac metamaterials), there is a novel topological phase transition, which corresponding to topological charges change from ± 2 to two ± 1 (see Appendix D). The evolution of the equal frequency contours are shown in Figs. 7(a)–7(d). In this process, the momentum sphere is split along the equator into two hyperboloids, and the Berry curvatures of the two hyperboloids are flipped, transforming into a degenerate two hyperboloid. Consequently, topological charges are equally split into half for each sheet as ± 1 and the symbol depends on different circular polarized light. For LCP, the reflected field across the interface show distinct topological features, two vortices with Chern number of -1 on both sides, and an unpredicted phase with topological charge being $+2$ emerges in the center, see in Fig. 7(e). Due to the mirror relationship of LCP and RCP, thus another case can be seen as a mirror operation and just flipped the corresponding Chern numbers, as shown in the Fig. 7(f). Namely, for the whole LCP or RCP, there ought to be a topological phase transition across the interface although the sum of Chern numbers vanishes. Under LCP or RCP excitation, the symmetry distributions of vortex structure and topological charge also clearly demonstrates the spin-momentum locking property in Dirac system. The excitation and propagation of robust spin-momentum wave demonstrated here may prove a different way of information transport and imaging applications.

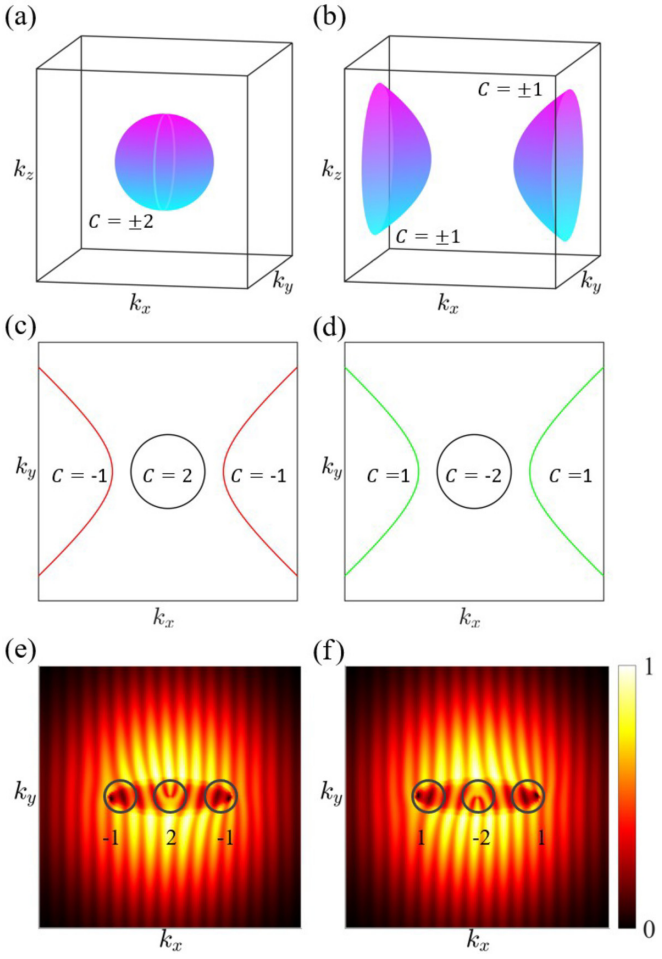

FIG. 7. Equifrequency contours of (a) isotropic system (air) and (b) Dirac metamaterials. In the transformation from air to degenerate Dirac metamaterials, the spin Chern numbers are split into ± 1. (c) and (d) represent the transition Chern numbers for spin up ($\sigma = 1$) and spin down ($\sigma = -1$) state in $k_x - k_y$ plane. (e) and (f) shows the interference patterns in left- and right-handed incident polarization respectively. For different spin input state, the reflected field occur the corresponding topological charge (Chern number) at Dirac points.

V. CONCLUSIONS

In conclusion, by considering electromagnetic duality symmetry of metamaterials with photonic Dirac point, we have developed a general model to describe the reflected state with Gaussian beam incidence and revealed the topological characteristics based on wave theory. When the beam impinges on the unique interface, we found that the original spin properties

have completely changed, and capture a vortex phase with nontrivial topological charge ±1. Moreover, we investigated the normal incidence of paired Dirac points, the reflecting field precisely not only show two vortices related to paired Dirac points, but also proved the topological charge for two points. These findings based on wave theory provide a different pathway to investigate and manipulate the polarization evolution with topological media and thereby open the possibility of developing various photonic devices. Our model can also be extended from the Dirac points to Weyl points and nodal lines in other 3D topological photonic systems with similar topological structure.

ACKNOWLEDGMENTS

This work is supported by the National Natural Science Foundation of China (Grants No. 11904097 and No. 61835004).

APPENDIX A: BAND STRUCTURE OF PHOTONIC DIRAC METAMATERIALS

The general permittivity and permeability tensors of Dirac metamaterials have the anisotropic form and we assume $\varepsilon_z = \varepsilon_y$, $\mu_z = \mu_y$ are constants. Note that the magnetoelectric tensors for the proposed metamaterials are not considered here, thus the detail of permittivity and permeability as follows:

$$\boldsymbol{\varepsilon} = \begin{vmatrix} \varepsilon_x & 0 & 0 \\ 0 & \varepsilon_y & 0 \\ 0 & 0 & \varepsilon_y \end{vmatrix}, \qquad \boldsymbol{\mu} = \begin{vmatrix} \mu_x & 0 & 0 \\ 0 & \mu_y & 0 \\ 0 & 0 & \mu_y \end{vmatrix}, \tag{A1}$$

where ε_x and μ_x indicates the resonance along the x direction that there exist two bulk plasmon modes, a longitudinal electric mode and a longitudinal magnetic mode, $\varepsilon_x = 1 + f_1\,\omega_0^2/(\omega_0^2 - \omega^2)$, $\mu_x = 1 + f_2\,\omega^2/(\omega_0^2 - \omega^2)$, where ω_0 indicates the resonance frequency and coefficients f_1 and f_2 are constants determined by the structure parameters, which are adjustable [1].

To gain the band structure of photonic Dirac metamaterials, we treat the combined electric field $\mathbf{E} = (E_x, E_y, E_z)$ and magnetic field $\mathbf{H} = (H_x, H_y, H_z)$ as two three-component vectors, and using the relations in Maxwell's equation:

$$\nabla \times \mathbf{E} = i\omega\mathbf{B}, \tag{A2}$$

$$\nabla \times \mathbf{H} = -i\omega\mathbf{D}. \tag{A3}$$

Considering the constitutive relations: $\mathbf{D} = \varepsilon_0\boldsymbol{\varepsilon}\mathbf{E}$, $\mathbf{B} = \mu_0\boldsymbol{\mu}\mathbf{H}$, and multiply $\nabla \times \boldsymbol{\mu}^{-1}$ on both sides of (A2), we get:

$$\nabla \times \boldsymbol{\mu}^{-1}\nabla \times \mathbf{E} - \omega^2\boldsymbol{\varepsilon}\mathbf{E} = 0. \tag{A4}$$

Likewise, For (A3), we get the similar equation:

$$\nabla \times \boldsymbol{\varepsilon}^{-1}\nabla \times \mathbf{H} - \omega^2\boldsymbol{\mu}\mathbf{H} = 0, \tag{A5}$$

which are regarded as the wave equations for anisotropic media. Assuming that $\mathbf{E}$ and $\mathbf{H}$ are of the form $e^{i\mathbf{k}\cdot\mathbf{r}}$, thus $\mathbf{k}\times$ are used in place of $\nabla\times$.

$$\mathbf{k}\times \equiv \begin{vmatrix} 0 & -k_z & k_y \\ k_z & 0 & -k_x \\ -k_y & k_x & 0 \end{vmatrix}. \tag{A6}$$

The wave equations are rewritten as $\mathbf{M}\cdot\mathbf{E} = 0$ and $\mathbf{N}\cdot\mathbf{H} = 0$, where

$$\mathbf{M} = \mathbf{k}\times\mathbf{I}\,\mu^{-1}\,\mathbf{k}\times\mathbf{I} + \omega^2\boldsymbol{\varepsilon}, \tag{A7}$$

$$\mathbf{N} = \mathbf{k}\times\mathbf{I}\,\varepsilon^{-1}\,\mathbf{k}\times\mathbf{I} + \omega^2\boldsymbol{\mu}, \tag{A8}$$

with $\mathbf{I}$ being the identity tensor. The zero determinant of $\mathbf{M}(\mathbf{N})$ can gives rise to the characteristic equation, and dispersion relations are directly solved by the characteristic equation with the electromagnetic parameters (A1), the band structure of Dirac metamaterials can be deduced, as shown in Fig. 1(a).

APPENDIX B: CALCULATION OF THE FRESNEL COEFFICIENTS IN DIRAC METAMATERIALS

In this part, we show the detailed deducing process of reflection coefficients near the photonic Dirac point. Based on Maxwell equations and boundary conditions, we can derive the general Fresnel reflection coefficients with the permittivity tensor Eqs. (2) and (3) The reflection of arbitrary wave vector can be indicated by α from the result, when $\alpha = 0$ the permittivity tensors are degenerate to the original diagonal form.

For a given incident wave vector $\boldsymbol{k}_i = (k_x, 0, k_z)$, there are two normal (to the interface) wave vectors components by solve the characteristic equation from the constitutive relations and Maxwell's equations:

$$k_z^- = \sqrt{\frac{-k_x^2(\alpha^2\delta\varepsilon + \varepsilon_y) + k^2\varepsilon_x\varepsilon_y\mu_y}{\varepsilon_y}}, \tag{B1}$$

$$k_z^+ = \sqrt{\frac{-k_x^2(\alpha^2\delta\mu + \mu_y) + k^2\varepsilon_x\mu_y\mu_x}{\mu_y}}, \tag{B2}$$

where superscripts + and − denote the two different modes, respectively.

Those two normal (to the interface) wave vectors components are associated with eigenwaves determined by the null space of Hamiltonian formalism, given as $\mathbf{E}^{\pm} = E_0(e_x^{\pm}, e_y^{\pm}, e_z^{\pm})$, where E_0 are the electric field magnitudes for the plus and minus modes, respectively.

$$\begin{vmatrix} e_x^- \\ e_y^- \\ e_z^- \end{vmatrix} = \begin{vmatrix} \cos\alpha(k_x^2 - k^2\varepsilon_o\mu_o) \\ -\sin\alpha k^2\varepsilon_o\mu_o \\ \cos\alpha k_x k_z^- \end{vmatrix}, \tag{B3}$$

$$\begin{vmatrix} e_x^+ \\ e_y^+ \\ e_z^+ \end{vmatrix} = \begin{vmatrix} -\sin\alpha k_z^+ \\ \cos\alpha k_z^+ \\ \sin\alpha k_x \end{vmatrix}. \tag{B4}$$

Likewise the corresponding magnetic fields are also obtained by constitutive relation, $\mathbf{H}^{\pm} = \omega^{-1}\mu^{-1}k \times \mathbf{E}^{\pm} = \frac{E_0}{\eta_0}(h_x^{\pm}, h_y^{\pm}, h_z^{\pm})$, where $\eta_0 = \sqrt{\mu_0/\varepsilon_0}$.

$$\begin{vmatrix} h_x^- \\ h_y^- \\ h_z^- \end{vmatrix} = k\varepsilon_o \begin{vmatrix} \sin\alpha k_z^- \\ -\cos\alpha k_z^- \\ -\sin\alpha k_x \end{vmatrix},$$

$$\begin{vmatrix} h_x^+ \\ h_y^+ \\ h_z^+ \end{vmatrix} = \frac{1}{k\mu_o} \begin{vmatrix} \cos\alpha(k_x^2 - k^2\varepsilon_o\mu_o) \\ -\sin\alpha k^2\varepsilon_o\mu_o \\ \cos\alpha k_x k_z^+ \end{vmatrix}. \tag{B5}$$

The reflection and refraction on the interface of Dirac metamaterials can be described with Fresnel's equations and

boundary conditions. Fresnel's reflection coefficients are determined by the incident and reflected amplitudes: $r_{pp} = E_r^p/E_i^p$, $r_{ss} = E_r^s/E_i^s$, $r_{ps} = E_r^p/E_i^s$, and $r_{sp} = E_r^s/E_i^p$, and the general reflection coefficients can be obtained as

$$r_{pp} = \frac{s_{xx} - s_{yy}\cos^2\theta + (-e_{xy} + h_{xy})\cos\theta}{s_{xx} + s_{yy}\cos^2\theta - (e_{xy} + h_{xy})\cos\theta}, \tag{B6}$$

$$r_{ss} = \frac{-s_{xx} + s_{yy}\cos^2\theta + (-e_{xy} + h_{xy})\cos\theta}{s_{xx} + s_{yy}\cos^2\theta - (e_{xy} + h_{xy})\cos\theta}, \tag{B7}$$

$$r_{ps} = \frac{2s_{xy}\cos^2\theta}{s_{xx} + s_{yy}\cos^2\theta - (e_{xy} + h_{xy})\cos\theta}, \tag{B8}$$

$$r_{sp} = \frac{2s_{yx}\cos^2\theta}{s_{xx} + s_{yy}\cos^2\theta - (e_{xy} + h_{xy})\cos\theta}, \tag{B9}$$

with $s_{ij} = e_i^+ h_j^- - e_i^- h_j^+$, $e_{ij} = e_i^+ e_j^- - e_i^- e_j^+$, $h_{ij} = h_i^+ h_j^- - h_i^- h_j^+$ and $\{i, j\} = \{x, y\}$, respectively.

APPENDIX C: REFLECTION FIELD NEAR THE SINGLE PHOTONIC DIRAC POINTS

Near the Dirac point, the center vector of incident beam can be regarded as $\boldsymbol{k_i} = (k\sin\theta_i, 0, k\cos\theta_i)$, while the arbitrary wave vector can be indicated by α. By using the paraxial approximation, $\cos\alpha \to 1$, $\sin\alpha \sim \frac{k_{iy}}{k\sin\theta}$, the transverse component of arbitrary wave vector were considered, the modified Fresnel coefficients of oblique incident are given as follows [33]:

$$r_{pp} = \frac{-Q + \sqrt{\varepsilon_x\varepsilon_y}\cos\theta}{Q + \sqrt{\varepsilon_x\varepsilon_y}\cos\theta}, \tag{C1}$$

$$r_{ss} = \frac{-Q + \sqrt{\mu_x\mu_y}\cos\theta}{Q + \sqrt{\mu_x\mu_y}\cos\theta}, \tag{C2}$$

$$r_{ps} = \frac{2\frac{k_{iy}}{k\sin\theta}\sqrt{\varepsilon_y\mu_y}(\sqrt{\varepsilon_x\mu_x} - \sqrt{\varepsilon_y\mu_y})\cos\theta}{(Q + \sqrt{\varepsilon_x\varepsilon_y}\cos\theta)(Q + \sqrt{\mu_x\mu_y}\cos\theta)}, \tag{C3}$$

$$r_{sp} = \frac{2\frac{k_{iy}}{k\sin\theta}\sqrt{\varepsilon_y\mu_y}(\sqrt{\varepsilon_y\mu_y} - \sqrt{\varepsilon_x\mu_x})\cos\theta}{(Q + \sqrt{\varepsilon_x\varepsilon_y}\cos\theta)(Q + \sqrt{\mu_x\mu_y}\cos\theta)}, \tag{C4}$$

where $Q = \sqrt{\varepsilon_y\mu_y - \sin^2\theta}$, r_{pp}, r_{ss}, r_{ps} and r_{sp} denote the Fresnel reflection coefficients for parallel, perpendicular and crossing polarizations, respectively. When $\varepsilon_x = \varepsilon_y = const$, $\boldsymbol{\mu} = 1$, the reflection coefficients can reproduce to the Fresnel equation in the classic case of isotropic [38].

To obtain a precise model of Gaussian beam, the arbitrary wave vector along x also needs to be taken into account. By making use of Taylor series expansion, the reflection coefficients are expanded as a polynomial of k_{ix}, and higher-order terms have a negligible influence in paraxial transmission [39]. Hence, these moduli of reflection matrix can be written as follows:

$$\begin{bmatrix} r_{xx} & r_{xy} \\ r_{yx} & r_{yy} \end{bmatrix} = \begin{bmatrix} r_{pp} - \frac{k_{rx}}{k}r'_{pp} & \frac{k_{ry}}{k}r'_{ps} \\ \frac{k_{ry}}{k}r'_{sp} & r_{ss} - \frac{k_{rx}}{k}r'_{ss} \end{bmatrix}, \tag{C5}$$

where $r'_{pp} = \partial r_{pp}/\partial\theta$, $r'_{ss} = \partial r_{ss}/\partial\theta$, $r_{sp} = r'_{sp}k_{ry}/k$, and $r_{ps} = r'_{ps}k_{ry}/k$. In the above equation, the boundary conditions $k_{rx} = -k_{ix}$ and $k_{ry} = k_{iy}$ have been introduced and ∂k_{rx} can be replaced with $k\partial\theta$. The polarizations associated with the angular spectrum components experience different rotations in order to satisfy the transversality of photon polarization after reflection. So far, we give the specific form of the above Fresnel reflection matrix, which retains robustness and accuracy and can be used in other similar bulk materials based on a real Gaussian beam transmission.

In Figs. 3(a) and 3(b), the diagonal elements for Fresnel reflection matrix are plotted as a function of incident angle θ. By tuning the geometric parameters of the Dirac metamaterials, we set the $\theta = 30^\circ$ as the incident condition of Dirac point. It can be seen that maximum amplitude of the four coefficients exists near Dirac point and $r_{pp} = r_{ss}$, $r'_{pp} = r'_{ss}$, which means $r_{xx} = r_{yy}$ at critical angle. For more general cases, we transform the matrix into circular polarization basis. Thus, the reflected polarization states related to the incident left-handed and right-handed polarization states can be described by the following matrix:

$$\begin{bmatrix} \tilde{E}_r^+ \\ \tilde{E}_r^- \end{bmatrix} = \begin{bmatrix} r_{ll} & r_{lr} \\ r_{rl} & r_{rr} \end{bmatrix} \cdot \begin{bmatrix} \tilde{E}_i^+ \\ \tilde{E}_i^- \end{bmatrix}, \tag{C6}$$

where $|+\rangle$ and $|-\rangle$ represent the left- and right-handed circular polarization components, respectively. From Eqs. (C1)–(C5), we can immediately derive the detail of Fresnel coefficient matrix under the CP basis [40].

$$r_{ll} = \tfrac{1}{2}[(r_{xx} - r_{yy}) - i(r_{xy} + r_{yx})], \tag{C7}$$

$$r_{rr} = \tfrac{1}{2}[(r_{xx} - r_{yy}) + i(r_{xy} + r_{yx})], \tag{C8}$$

$$r_{lr} = \tfrac{1}{2}[(r_{xx} + r_{yy}) - i(r_{xy} - r_{yx})], \tag{C9}$$

$$r_{rl} = \tfrac{1}{2}[(r_{xx} + r_{yy}) + i(r_{xy} - r_{yx})]. \tag{C10}$$

Obviously, Eqs. (C7)–(C10) show that for reflection near the Dirac point, two components $r_{ll} = r_{rr} = 0$ do not supply any phase and contribute to reflections, while the other two components r_{lr} and r_{rl} carry the vortex phase information, as shown in Figs. 3(c) and 3(d) in main text. The higher-order Poincaré can be derived naturally from the fundamental Poincaré sphere.

APPENDIX D: CALCULATION OF BERRY PHASE AND TOPOLOGICAL CHARGE

We first give the topological charge of origin media, and we can derive the eigenstates under spherical coordinate as:

$$|\psi(\mathbf{R})\rangle = \frac{\sqrt{2}}{2}\begin{bmatrix} -\cos\alpha\cos\vartheta + \sigma i\sin\alpha \\ -\sin\alpha\cos\vartheta - \sigma i\cos\alpha \\ \sin\vartheta \end{bmatrix}, \tag{D1}$$

where ϑ and α are the polar angle and azimuthal angle, respectively, $\sigma = \pm 1$ represents the spin of LCP or RCP. Then we can easily derive the corresponding Berry connection from definition [41].

$$\mathbf{A} = i\langle\psi(\mathbf{R})|\nabla_{\mathbf{R}}|\psi(\mathbf{R})\rangle = \sigma\cos\vartheta, \tag{D2}$$

and the Berry phase can be written as:

$$\gamma_\sigma = \int_0^{2\pi}\mathbf{A}d\alpha = \sigma 2\pi\cos\vartheta, \tag{D3}$$

when the polar angle $\vartheta = 0$, the integral area of Berry curvature is zero and the Berry phase is just zero. So, Eq. (D3) can

be rewritten as:

$$\gamma_\sigma = -2\pi\sigma(1-\cos\vartheta). \tag{D4}$$

Owing to the transverse nature of electromagnetic waves, the propagation of light in free space possesses Berry curvature in the momentum space given by

$$\mathbf{\Omega} = \sigma\mathbf{k}/|\mathbf{k}|^3. \tag{D5}$$

By calculating the integral of above Berry curvature on k sphere, corresponding Chern number can be obtained as follows:

$$C_\sigma = \frac{1}{2\pi}\int_0^{2\pi}\int_0^{\pi}\sigma\frac{\mathbf{k}}{2|\mathbf{k}|^3}dS = 2\sigma. \tag{D6}$$

Next, we show the topological charge around the paired Dirac points from effective Hamiltonian [1,4].

$$H_\sigma = \begin{bmatrix} k_x & \frac{1}{2}(k_z - i\sigma k_y) \\ \frac{1}{2}(k_z + i\sigma k_y) & 0 \end{bmatrix}. \tag{D7}$$

Similar to the previously proposed case, for eigenstate $|\psi(k)\rangle$

$$|\psi(\mathbf{k})\rangle = \begin{bmatrix} k_x \pm k \\ k_z - i\sigma k_y \end{bmatrix}, \tag{D8}$$

we may define a "gauge potential" as

$$a_i(\mathbf{k}) = -i\langle\psi(\mathbf{k})|\frac{\partial}{\partial k_i}|\psi(\mathbf{k})\rangle, \tag{D9}$$

and the Berry curvature for Dirac points in momentum space is given by

$$\mathbf{\Omega_D} = \frac{\partial}{\partial k_y}a_x(\mathbf{k}) - \frac{\partial}{\partial k_x}a_y(\mathbf{k}). \tag{D10}$$

The topological charge (Chern number) is the integral of the Berry curvature $\vec{\Omega}_D$ over the Brillouin zone. By substituting the vector relationship of Dirac point into the above Berry curvature and integral expressions, we can obtain the topological charge as follows:

$$C_\sigma = \frac{1}{2\pi}\int_0^{2\pi}\int_0^{\pi}\sigma\frac{\mathbf{k}}{2|\mathbf{k}|^3}dS = -\sigma. \tag{D11}$$

The above results accurately coincide with the topological charge of vortex polarized beam under spin-up ($\sigma = +1$, LCP) and spin-down ($\sigma = -1$, RCP) input state, respectively.

[1] Q. Guo, B. Yang, L. Xia, W. Gao, H. Liu, J. Chen, Y. Xiang, and S. Zhang, Phys. Rev. Lett. **119**, 213901 (2017).

[2] Q. Guo, O. You, B. Yang, J. B. Sellman, E. Blythe, H. Liu, Y. Xiang, J. Li, D. Fan, J. Chen, C. T. Chan, and S. Zhang, Phys. Rev. Lett. **122**, 203903 (2019).

[3] L. Lu, Z. Wang, D. Ye, L. Ran, L. Fu, J. D. Joannopoulos, and M. Soljačić, Science **349**, 622 (2015).

[4] W. Gao, B. Yang, M. Lawrence, F. Fang, B. Béri, and S. Zhang, Nature Commun. **7**, 12435 (2016).

[5] M. Xiao, Q. Lin, and S. Fan, Phys. Rev. Lett. **117**, 057401 (2016).

[6] J. Noh, S. Huang, D. Leykam, Y. D. Chong, K. P. Chen, and M. C. Rechtsman, Nature Phys. **13**, 611 (2017).

[7] B. Yang, Q. Guo, B. Tremain, L. E. Barr, W. Gao, H. Liu, B. Béri, Y. Xiang, D. Fan, A. P. Hibbins, and S. Zhang, Nature Commun. **8**, 97 (2017).

[8] L. Lu, L. Fu, J. D. Joannopoulos, and M. Soljačić, Nature Photonics. **7**, 294 (2013).

[9] L. Tarruell, D. Greif, T. Uehlinger, G. Jotzu, and T. Esslinger, Nature (London) **483**, 302 (2012).

[10] G. Jotzu, M. Messer, R. Desbuquois, M. Lebrat, T. Uehlinger, D. Greif, and T. Esslinger, Nature (London) **515**, 237 (2014).

[11] D. Torrent and J. Sánchez-Dehesa, Phys. Rev. Lett. **108**, 174301 (2012).

[12] M. Xiao, G. Ma, Z. Yang, P. Sheng, Z. Zhang, and C. Chan, Nature Phys. **11**, 240 (2015).

[13] G. Ma, M. Xiao, and C. T. Chan, Nature Rev. Phys. **1**, 281 (2019).

[14] Y. Yang, Z. Gao, H. Xue, L. Zhang, M. He, Z. Yang, R. Singh, Y. Chong, B. Zhang, and H. Chen, Nature (London) **565**, 622 (2019).

[15] T. Ozawa, H. M. Price, A. Amo, N. Goldman, M. Hafezi, L. Lu, M. C. Rechtsman, D. Schuster, J. Simon, O. Zilberberg, and I. Carusotto, Rev. Mod. Phys. **91**, 015006 (2019).

[16] L. Lu, J. D. Joannopoulos, and M. Soljačić, Nature Phys. **12**, 626 (2016).

[17] D. Han, Y. Lai, J. Zi, Z.-Q. Zhang, and C. T. Chan, Phys. Rev. Lett. **102**, 123904 (2009).

[18] G. Weick, C. Woollacott, W. L. Barnes, O. Hess, and E. Mariani, Phys. Rev. Lett. **110**, 106801 (2013).

[19] H. Cheng, W. Gao, Y. Bi, W. Liu, Z. Li, Q. Guo, Y. Yang, O. You, J. Feng, H. Sun, J. Tian, S. Chen, and S. Zhang, Phys. Rev. Lett. **125**, 093904 (2020).

[20] S. Barik, A. Karasahin, C. Flower, T. Cai, H. Miyake, W. DeGottardi, M. Hafezi, and E. Waks, Science **359**, 666 (2018).

[21] X. T. He, E. T. Liang, J. J. Yuan, H. Y. Qiu, X. D. Chen, F. L. Zhao, and J. W. Dong, Nature Commun. **10**, 872 (2019).

[22] Z. Q. Yang, Z. K. Shao, H. Z. Chen, X. R. Mao, and R. M. Ma, Phys. Rev. Lett. **125**, 013903 (2020).

[23] G. Milione, H. I. Sztul, D. A. Nolan, and R. R. Alfano, Phys. Rev. Lett. **107**, 053601 (2011).

[24] A. Holleczek, A. Aiello, C. Gabriel, C. Marquardt, and G. Leuchs, Opt. Express **19**, 9714 (2011).

[25] G. Milione, S. Evans, D. A. Nolan, and R. R. Alfano, Phys. Rev. Lett. **108**, 190401 (2012).

[26] X. Wang, Z. Nie, Y. Liang, J. Wang, T. Li, and B. Jia, Nanophotonics **7**, 1533 (2018).

[27] S. Chen, X. Zhou, Y. Liu, X. Ling, H. Luo, and S. Wen, Opt. Lett. **39**, 5274 (2014).

[28] Y. Liu, X. Ling, X. Yi, X. Zhou, H. Luo, and S. Wen, Appl. Phys. Lett. **104**, 191110 (2014).

[29] X. Yi, Y. Liu, X. Ling, X. Zhou, Y. Ke, H. Luo, S. Wen, and D. Fan, Phys. Rev. A **91**, 023801 (2015).

[30] A. B. Khanikaev, S. Hossein Mousavi, W.-K. Tse, M. Kargarian, A. H. MacDonald, and G. Shvets, Nature Mater. **12**, 233 (2013).
[31] A. Slobozhanyuk, S. H. Mousavi, X. Ni, D. Smirnova, Y. S. Kivshar, and A. B. Khanikaev, Nature Photonics. **11**, 130 (2017).
[32] J. Lekner, J. Phys.: Condens. Matter **3**, 6121 (1991).
[33] W. Xu, Q. Yang, G. Ye, W. Wu, W. Zhang, H. Luo, and S. Wen, Phys. Rev. A **101**, 023826 (2020).
[34] Q. Yang, W. Xu, S. Chen, S. Wen, and H. Luo, Phys. Rev. A **103**, 023522 (2021).
[35] X. Ling, W. Xiao, S. Chen, X. Zhou, H. Luo, and L. Zhou, Phys. Rev. A **103**, 033515 (2021).
[36] K. S. Novoselov, A. K. Geim, S. V. Morozov, D. Jiang, M. I. Katsnelson, I. V. Grigorieva, S. V. Dubonos, and A. A. Firsov, Nature (London) **438**, 197 (2005).
[37] Y. Zhang, Y.-W. Tan, H. L. Stormer, and P. Kim, Nature (London) **438**, 201 (2005).
[38] M. Born and F. Wolf, *Principles of Optics: Electromagnetic Theory of Propagation, Interference and Diffraction of Light* (Elsevier, Amsterdam, 2013).
[39] H. Luo, X. Zhou, W. Shu, S. Wen, and D. Fan, Phys. Rev. A **84**, 043806 (2011).
[40] H. Xu, G. Wang, T. Cai, J. Xiao, and Y. Zhang, Opt. Express **24**, 27836 (2016).
[41] M. V. Berry, Proc. R. Soc. London, Ser. A **392**, 45 (1984).